ARTICLE

Exploring the Mechanical Properties, Shrinkage and Compensation Mechanism of Cement Stabilized Macadam-Steel Slag from Multiple Perspectives

Wei Zhang[1], Mulian Zheng[1,*], Yifeng Li[2] and Wuxi Zheng[3]

[1]Key Laboratory for Special Area Highway Engineering of Ministry of Education, Chang'an University, Xi'an, 710064, China

[2]Rizhao Transportation Management Center, Rizhao, 27680, China

[3]Central-South Safety & Environment Technology Institute Co., Ltd., Wuhan, 43000, China

[*]Corresponding Author: Mulian Zheng. Email: zhengml@chd.edu.cn

ABSTRACT

Steel slag is characterized by high strength, good wear resistance and micro-expansion. This study aims at exploring the potential of steel slag in cement stabilized aggregates, mainly including mechanical properties, shrinkage and compensation mechanisms. For this purpose, the compressive strength and compressive resilient modulus of cement stabilized aggregates with different steel slag contents (CSMS) were initially investigated. Subsequently, the effects of steel slag and cement on dry shrinkage, temperature shrinkage, and total shrinkage were analyzed through a series of shrinkage test designs. Additionally, in combination with X-ray diffraction (XRD) and Scanning electron microscope (SEM), the characteristic peaks and microscopic images of cement, steel slag and cement-steel slag at different hydration ages were analyzed to identify the chemical substances causing the expansion volume of steel slag and reveal the compensation mechanism of CSMS. The results show that the introduction of 20% steel slag improved the mechanical properties of CSMS by 16.7%, reduced dry shrinkage by 21%, increased temperature shrinkage by 5.8% and reduced its total shrinkage by 19.2%. Compared with the hydration reaction of cement alone, the composite hydration reaction of steel slag with cement does not produce new hydrates. Furthermore, it is noteworthy that the volume expansion of the f-CaO hydration reaction in steel slag can compensate for the volume shrinkage of cement-stabilized macadam. This research can provide a solid theoretical basis for the application and promotion of steel slag in cement-stabilized macadam and reduce the possibility of shrinkage cracking.

KEYWORDS

Cement stabilized macadam-steel slag; compensate; mechanical properties; pavement base; shrinkage; steel slag

1 Introduction

Steel slag is a by-product of the steel industry mainly composed of silica, magnesium oxide, calcium oxide, aluminum and iron [1,2]. After generation, steel slag is intended to be disposed of in landfills, not only occupying massive land but also destroying the ecological environment due to the leakage of harmful components [3,4]. Due to the excellent wear resistance, high strength and hardness, the reuse of steel slag as a complete or partial substitute for aggregates can improve the environmental effect and is therefore of great interest in practice and research [5,6]. As for the supply of aggregates, it is increasingly

difficult to obtain high-quality aggregates in many regions of the world due to environmental protection policy requirements and mining restrictions [7,8]. Thereafter, the use of steel slag instead of mineral materials has a huge demand prospect in engineering applications, especially in the field of road construction.

The United States, Japan, Germany and other developed countries have conducted extensive research on the use of steel slag and formed a systematic and stable application of specifications in road engineering. Most of the steel slag can be recycled and used for road bases, with the utilization rate being over 80% [9–11]. In China, the research on steel slag started late. Although there are some applications in road subgrade, micro-surface, gravel seal, and surface layer, it lacks a certain depth and fails to form a more unified system specification. So the application and promotion scope is relatively small [12,13].

Steel slag is widely used in road bases with low moisture exposure due to its porous nature and water absorption [14,15]. Maslehuddin et al. [16] applied steel slag to cement stabilized aggregates and declared that the mechanical properties of CMSM were superior to those of ordinary semi-rigid bases. Netinger et al. [17] announced that replacing partly coarse aggregates with larger-size steel slag could significantly improve the compressive strength, elastic modulus, and durability of cement concrete. In the shrinkage study of steel slag, Wang et al. [18] proposed a method to solve its expansion issue and a grading formula applicable to steel slag base material, thus establishing the relationship between void ratio and expansion rate. Due to the changes in temperature and humidity, cement stabilized aggregates are prone to volume shrinkage, resulting in shrinkage cracking in the roadbed, which seriously damages road performance [19–21]. Using the expansion property of steel slag to compensate for the shrinkage of cement-stabilized macadam has been a research hotspot in recent years [22,23]. Liu et al. [5] conducted a feasibility study on the application of steel slag in road subgrade and determined the optimum aggregate dosage. The results showed that steel slag performed well in improving the mechanical strength and shrinkage resistance of cement stabilized aggregates, and the optimal dosage of cement and steel slag were 4% and 50%, separately. Li et al. [24] investigated the dry shrinkage and temperature shrinkage of CMS and confirmed that the use of steel slag instead of aggregates could reduce the dry shrinkage and temperature shrinkage of semi-rigid base materials. Numerous studies on CSMS have demonstrated that its mechanical properties and shrinkage resistance are better than those of ordinary cement aggregates [25,26]. However, the current research is mainly focused on temperature shrinkage or dry shrinkage, while fewer studies have been done on dry-temperature comprehensive shrinkage, which is inconsistent with the actual application environment. Moreover, the studies of shrinkage mainly consider the dosage of steel slag or cement and lack the analysis of the shrinkage compensation mechanism from the microscopic perspective.

Consequently, based on the above issues, the objective of this study is to investigate the mechanical properties, shrinkage and shrinkage compensation mechanisms of CMS. To achieve this goal, a series of laboratory tests are conducted to explore the temperature shrinkage, dry shrinkage and dry-temperature comprehensive shrinkage of CMS with different steel slag and cement contents. Additionally, the crystalline phase, micrographs and hydration products of CMS are analyzed by XRD and SEM techniques to reveal its expansion compensation mechanism.

2 Materials and Methods

2.1 Materials

In this study, P·O 42.5 cement was used. Its properties and chemical components are shown in Tables 1 and 2, respectively. The mineral aggregates were limestone. According to the Test Methods of Aggregate for Highway Engineering (hereafter named JTG E42-2005), the properties such as mineral density, water absorption and crushing value were tested, and the values are shown in Table 3. The steel slag (see Fig. 1) used was taken from the Rizhao Steel Mill and has been stably treated by a thermal sedimentation process. Fig. 2 shows the SEM image of steel slag, from which it can be found that its surface is uneven

and porous. The natural grading curve of steel slag can be obtained by a sieving test, as shown in Table 4. Its properties and chemical compositions are shown in Tables 2 and 3 separately.

Table 1: Properties of P·O 42.5 cement

Test items		Technical requirements	Test results
Fineness (%)		≤10.0	2.3
Stability (mm)		≤5.0	1.5
Setting time (min)	Initial setting time	≥45	246
	Final setting time	≤600	458
Compressive strength (MPa)	3 d	≥17.0	24.8
	28 d	≥42.5	47.5
Flexural strength (MPa)	3 d	≥3.5	4.9
	28 d	≥6.5	7.7

Table 2: Chemical components of P·O 42.5 cement and steel slag

Sample	Components (%)							
	CaO	SiO_2	Al_2O_3	SO_3	Fe_2O_3	MgO	T-Fe	Others
Cement	58.44	23.61	6.04	2.18	3.35	1.91	–	4.47
Steel slag	38.29	14.03	2.92	–	30.33	8.12	2.42	3.89

Table 3: Properties of aggregate and steel slag

Test items		Aggregate	Steel slag	Technical requirements
4.75~16 mm	Apparent density (g/cm³)	2.725	3.248	≥2.6
	Water absorption (%)	0.71	1.3	≤2
2.36~4.75 mm	Apparent density (g/cm³)	2.733	3.281	≥2.6
	Water absorption (%)	0.94	1.7	≤2
Crushing value (%)		19.3	13.2	≤22
Los Angeles abrasion value (%)		15.2	17.4	≤26
Needle flake content of coarse aggregate (%)		12.1	2.1	≤18
Content with particle size less than 0.075 mm (%)		1.9	2.4	≤1.0

2.2 Mixing Proportion and Sample Preparation

2.2.1 Mixing Proportion

Discontinuous grading type C-B-3 was adopted for CMS, and the steel slag content was controlled by volume ratio. Through calculation, the gradation curves of CMS with 0%, 10%, 20% and 30% steel slag were shown in Fig. 3. Meanwhile, the proportion of aggregates for each grade with different steel slag contents are illustrated in Table 5.

Figure 1: Image of steel slag
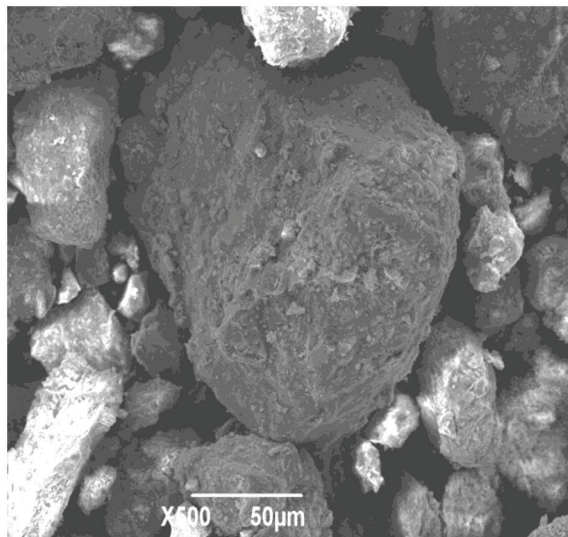
Figure 2: SEM image of steel slag

Table 4: Particle size of steel slag

Sieve size (mm)	Mass percentage through the following mesh (%)								
	13.2	9.5	4.75	2.36	1.18	0.60	0.30	0.15	0.075
Passing rate	95.86	85.36	51.30	25.40	16.30	11.10	6.60	4.94	3.40

2.2.2 Sample Preparation

The mixing process of CSMS is similar to that of ordinary cement stabilized macadam and the mixing equipment is a forced horizontal shaft mixer with the container of 0.06 L. Based on previous research experience, the mixing process of CSMS was presented below. ①: Weighing the mass of aggregates, steel slag, cement and water, respectively; ②: Adding the aggregates and steel slag to the mixer container and mixing for 5 min; ③: Adding the cement to the mixer container and mixing for 3 min; ④: Adding the

water to the mixer container and mixing for 5 min, the fresh CSMS was prepared; ⑤: According to the test requirements of optimal moisture content, dry density, mechanical properties and shrinkage, CSMS specimens with different sizes were formed and cured.
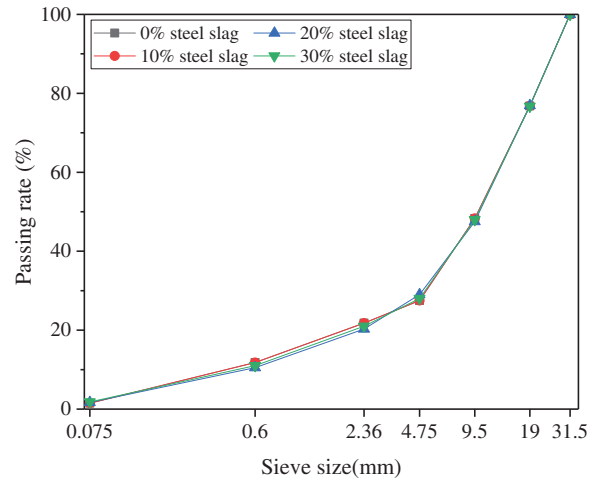
Figure 3: Grading curve of the mixtures with different steel slag contents

Table 5: Aggregates contents of each grade with different steel slag contents

Steel slag	20~30 mm	10~20 mm	5~10 mm	0~5 mm
0%	0	52%	21%	27%
10%	1%	50%	17%	22%
20%	2%	48%	11%	19%
30%	3%	45%	5%	17%

2.3 Experimental Methods

A series of laboratory experiments were conducted to investigate the shrinkage properties of CMS and reveal its shrinkage compensation mechanism. The research projects and methods are presented in Fig. 4. Firstly, the mechanical properties tests were conducted to verify the mechanical strength of CMS and the feasibility of engineering applications. Then, the effects of cement and steel slag contents on the shrinkage properties (dry shrinkage strain, temperature shrinkage strain and total shrinkage strain) of CMS were investigated by shrinkage test designs. Finally, XRD and SEM technologies were selected to study the properties of hydration products of cement and steel slag at different ages and reveal the shrinkage-expansion mechanism of CMS.

2.3.1 Optimal Moisture Content and Density

Table 3 shows that the density and water absorption of steel slag are different from that of aggregates. These properties of steel slag cause the CMS to exhibit different optimal moisture content and dry density depending on different steel slag contents. According to the Test Methods of Materials Stabilized with Inorganic Binders for Highway Engineering (hereafter named JTG E51-2009), the optimum moisture content and dry density of CMS with different steel slag and cement contents were investigated by heavy compaction tests. The results are presented in Figs. 5 and 6.
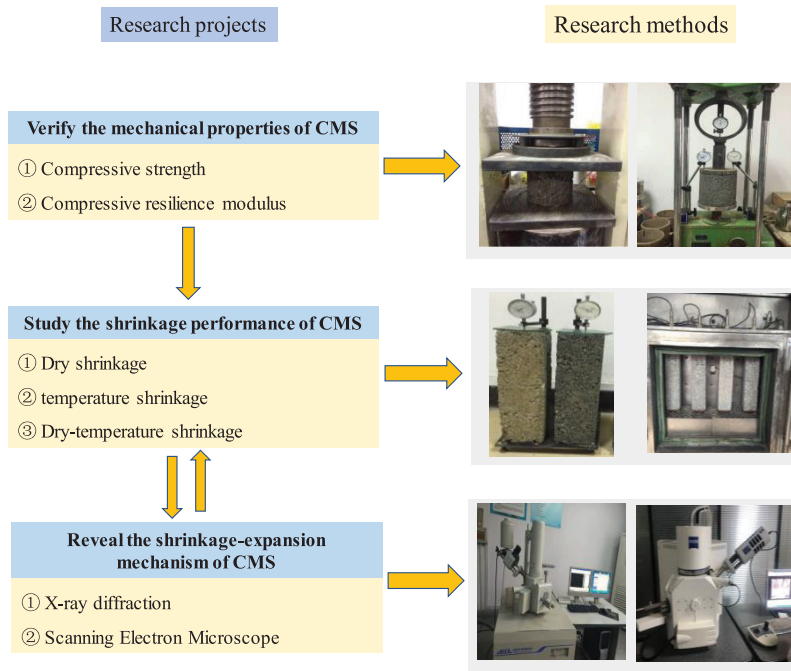
Figure 4: Research projects and methods
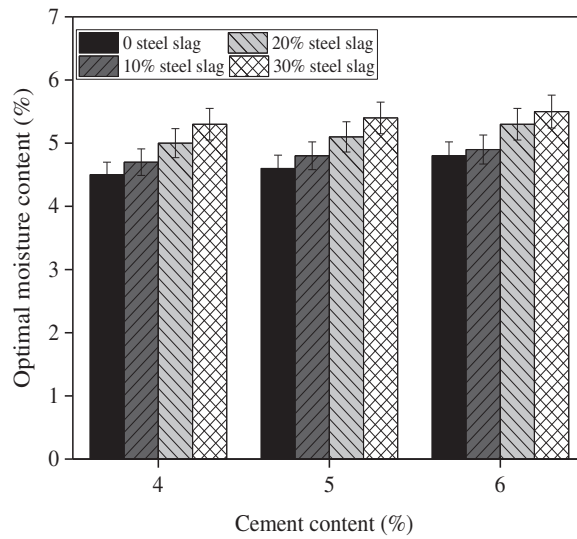
Figure 5: Optimal moisture content
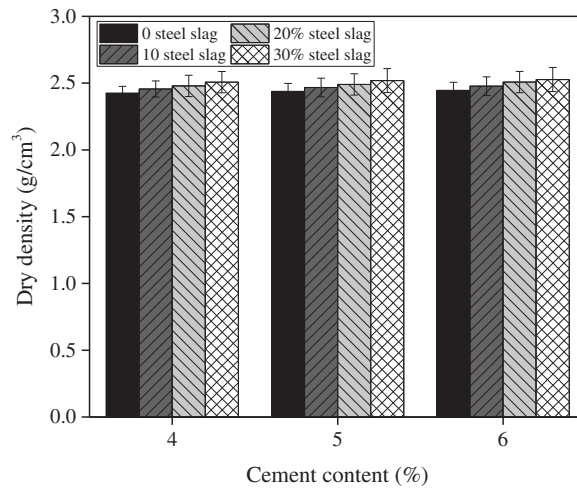
Figure 6: Dry density

2.3.2 Mechanical Properties

CMS is typically used in road subgrade to perform load-bearing functions. Therefore, it needs to have great compressive strength and compressive resilience modulus. In this study, 7 d unconfined compressive strength and 90 d compressive resilience modulus of CMS with different cement and steel slag contents were tested according to JTG E51-2009. The result is shown in Fig. 7.

(a) Compressive strength

(b) Compressive resilient modulus
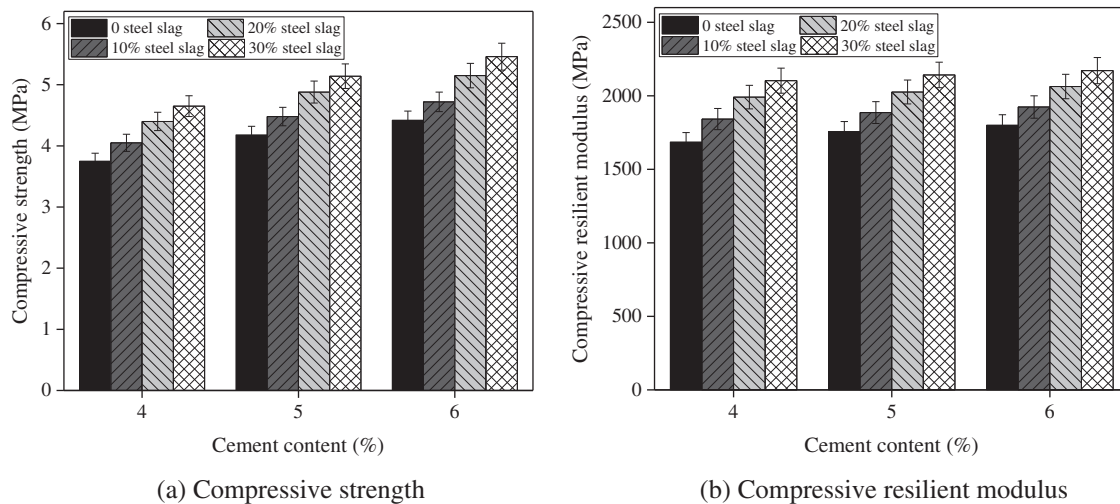
Figure 7: Mechanical properties of CMS with different steel slag and cement contents

2.3.3 Dry Shrinkage

The dry shrinkage of CMS was tested according to JTG E51-2009 (T0854). The size of the test specimen is 100 mm × 100 mm × 400 mm. The test temperature should be controlled at about 20°C, and the height of the specimen was recorded daily using a micrometer. Based on the test results, water loss and dry shrinkage strain of the specimens can be calculated according to Eqs. (1)–(3).

Water loss rate: $w_i = \dfrac{(m_i - m_{i+1})}{m_p}$ (1)

Dry shrinkage: $\delta_i = X_i - X_{i+1}$ (2)

Shrinkage strain: $\varepsilon_i = \dfrac{\delta_i}{l}$ (3)

where: w_i—The ith water loss rate (%);

　　　m_i—Weighing mass of the ith standard test piece (g);

　　　m_p—Mass of standard test piece after drying (g);

　　　δ_i—Dry shrinkage of the nth observation (mm);

　　　X_i—The value of the dial indicator at the ith test (mm);

　　　ε_i—The ith shrinkage strain (%);

　　　l—The length of the standard test piece (%).

2.3.4 Temperature Shrinkage

The temperature shrinkage test was conducted following JTG E51-2009 (T0855). The specimen of size 100 mm × 100 mm × 400 mm with 7 days curing age was used for the temperature shrinkage test. When the temperature rose to 40°C, data were collected and recorded at a frequency of 5 min/time. Thereafter, the temperature was cooled at a rate of 0.5 °C/min. When the temperature dropped to 30°C, it was held for 3 h, and then the temperature was reduced to −10°C as described above until the end of the test. The temperature shrinkage of the specimens could be obtained by a computer and the temperature shrinkage strain was calculated according to Eq. (4).

Temperature shrinkage strain: $\varepsilon_i = \dfrac{l_i - l_{i+1}}{L_0}$ (4)

where: ε_i—The average shrinkage strain at nth temperature (%);

　　　l_i—The displacement value of the ith temperature range (mm);

　　　L_0—The initial length of the test piece (mm).

2.3.5 Dry-Temperature Shrinkage

To conduct the dry-temperature shrinkage test, specimens need to contain moisture and be cured in a temperature-varying environment. The specimen of size 100 mm × 100 mm × 400 mm was used and the water curing age was 7 days. After drying their surface, the lengths of the specimens were measured. The subsequent operation is similar to the temperature shrinkage test. The total shrinkage was calculated according to Eq. (5).

Total shrinkage rate: $\delta = \dfrac{\Delta L}{L_0}$ (5)

where: δ—Total shrinkage rate (%);

　　　ΔL—Total shrinkage (mm);

　　　L_0—Length of the test piece (mm).

2.3.6 XRD

X-ray diffraction test is a commonly used phase analysis method, by which the diffraction pattern of the sample can be obtained. Combined with the position of the characteristic peak in the diffraction pattern, the material composition of the sample can be analyzed. After 7 and 28 days of hydration reaction, steel slag was dried and then ground into a powder with the maximum particle size of 0.075 mm. The diffraction intensity was measured by a Rigaku Ultimate IV X-ray diffractometer, using a Cu target with an operating voltage of

40 kV and a current of 40 mA. The sampling was performed in a continuous scanning mode with a scanning speed of 5°/min, a step size of 0.02, and a 2θ range of 10° to 70°.

2.3.7 SEM

SEM can observe the microscopic appearance of CMS through image scanning amplification technology. In this paper, SEM was used to observe the morphology of steel slag, cement slurry and steel slag-cement at different hydration ages. For this purpose, broken specimens with the size of 5 mm × 5 mm × 3 mm were collected after mechanical properties tests, then they were gold coated and SEM images were observed using a Zeiss Sigma 300 microscope.

3 Results and Discussions

3.1 Optimal Moisture Content and Density

Fig. 5 illustrates the result of optimal moisture content while Fig. 6 shows the result of density. From Figs. 5 and 6, it can be found that the optimum moisture content and dry density of CMS increased with the increase of cement contents for the same amount of steel slag. Likewise, with the increase of steel slag content, the optimal moisture content and dry density of CMS showed a similar growth trend. Compared with cement, steel slag has a greater influence on the optimal moisture content and dry density. This is because the water absorption and density of steel slag are larger than that of limestone aggregates. The more aggregates replaced with steel slag tended to endow CMS with higher optimal moisture content and dry density. This conclusion is consistent with Baalamurugan et al. [27] and Miah et al. [28]. For example, Baalamurugan et al. [27] declared that replacement of 40% as coarse aggregate and 100% as fine aggregate of steel slag in concrete increases the density and compressive strength of conventional concrete from 2.38 to 2.85 g/cm^3.

3.2 Mechanical Properties

Fig. 7 presents the mechanical properties of CMS with different steel slag and cement contents. Under the same cement content, higher steel slag content increased the 7 days compressive strength of CMS. Compared with CMS without steel slag, the 7 days compressive strength of CMS with 10%, 20% and 30% steel slag increased by 7.2%, 16.7% and 22.0%, respectively. Therefore, it can be concluded that the introduction of steel slag has a beneficial effect on the compressive strength. Meanwhile, the compressive resilient modulus of CMS exhibited a similar increasing trend with the increase of steel slag content. It can be interpreted that the active substances such as C_3S, C_2S in steel slag would participate in the hydration reaction and the products increased the mixture's denseness. Similar results were reported by Xiao et al. [29] and El-Didamony et al. [30]. Besides, the products also enhanced the adhesion between the aggregates and increased the strength and resilient modulus. Biskri et al. [31] announced that the best mechanical behavior obtained by HPC with steel slag aggregates was mainly due to the high strength of steel slag aggregates themselves and the cement paste-aggregates adhesion.

3.3 Dry Shrinkage

3.3.1 With Different Steel Slag Contents

Fig. 8 shows the water loss rate and dry shrinkage strain of CMS with different steel slag contents. It was noted that the water loss rate of CMS gradually increased with the increase of exposure time, and the rate of water loss was faster in the early stage. Especially in the first 7 days, the accumulative water loss accounted for 80%~90%. Likewise, an increase in steel slag content also led to an increase in the water loss of the CMS. Compared with CMS without steel slag, the accumulative water loss of CMS with 10%, 20% and 30% steel slag increased by 5.9%, 12.2% and 15.7%, respectively. This is because the water absorption rate of steel slag is large. After soaking, the higher content of steel slag led to elevated moisture of the CMS, resulting in a relative increase in water loss during the curing period. Therefore, CMS containing a large amount of

steel slag increased the total water loss rate. In terms of dry shrinkage strain (Fig. 8b), higher steel slag would reduce the dry shrinkage strain. Likewise, with the increase in exposure time, the dry shrinkage strain also increased gradually. An earlier study by Lim et al. [32] also concluded that the inclusion of steel slag tended to improve the mechanical strength of the concrete, while reducing the dry shrinkage.

(a) Water loss rate   (b) Dry shrinkage strain
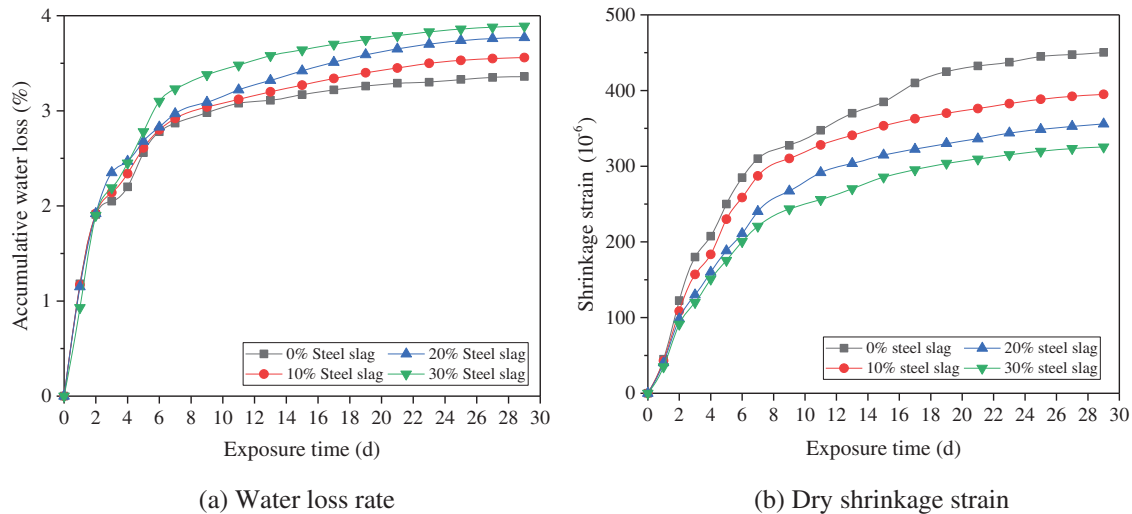
Figure 8: Dry shrinkage results of CMS with different steel slag contents

3.3.2 With Different Cement Contents

Fig. 9 gives the dry shrinkage results of CMS with different cement contents. It can be found in Fig. 9a that the accumulative water loss rate of CMS was negatively correlated with cement contents. That is, the cumulative water loss rate of CMS with 4%, 5% and 6% cement were 4.13%, 3.85% and 3.62%, respectively. Compared with CMS with 4% cement, the cumulative water loss rate of CMS with 5% and 6% cement decreased by 6.5% and 12.3% respectively indicating that higher cement content would reduce the accumulative water loss. With the increase of cement contents, the voids in the mixture gradually decreased, and the mixture tended to be denser. Additionally, as the exposure time increased, the hydration products produced by cement would gradually fill the voids. Thereafter, the mixture with higher cement content had smaller voids and greater density and absorbed less moisture when the specimens were immersed in water. While an important observation in Fig. 9b is that the dry shrinkage strain was positively correlated with the cement content, suggesting that an increase in cement content increased the dry shrinkage. In this case, although the total amount of water absorbed by the material decreased, the interlayer water in the material increased. When CMS was dried and shrunk, the volume shrinkage caused by adsorbed water, interlayer water and other bound water was greater than the free water in the voids, thereafter greater cement content would lead to a larger dry shrinkage strain.

3.4 Temperature Shrinkage

3.4.1 With Different Steel Slag Contents

Fig. 10 demonstrates the temperature shrinkage strain of CMS with different steel slag contents. As shown in Fig. 10, the temperature shrinkage strain of CMS decreased as the temperature decreased. While the higher content of steel slag caused an increase in temperature shrinkage strain. Compared with the CMS without steel slag, the temperature shrinkage strain of CMS with 10%, 20% and 30% steel slag increased by 2.3%, 5.8%, and 9.5%, respectively, which indicates that the incorporation of steel slag increased the temperature shrinkage strain, but the increased range was not significant. Among the CMS,

the temperature shrinkage strain is the largest for new products, followed by cement mortar, steel slag and limestone aggregate. That is, more hydration products correspond to a larger temperature shrinkage strain. The hydration reaction of active substances in steel slag increased the new products, so the temperature shrinkage strain of CMS was larger than that of common cement-stabilized macadam.

(a) Water loss rate   (b) Shrinkage strain
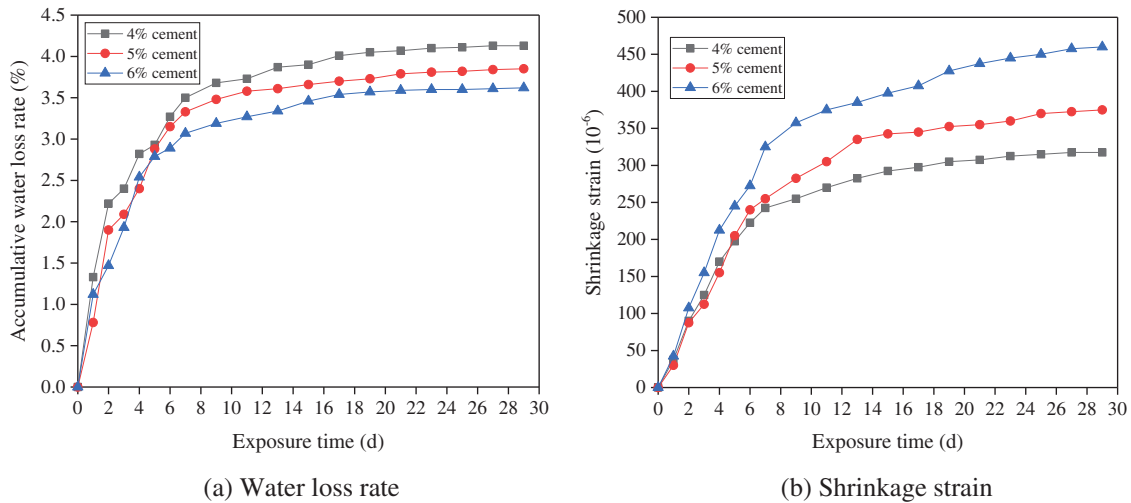
Figure 9: Dry shrinkage results of CMS with different cement contents
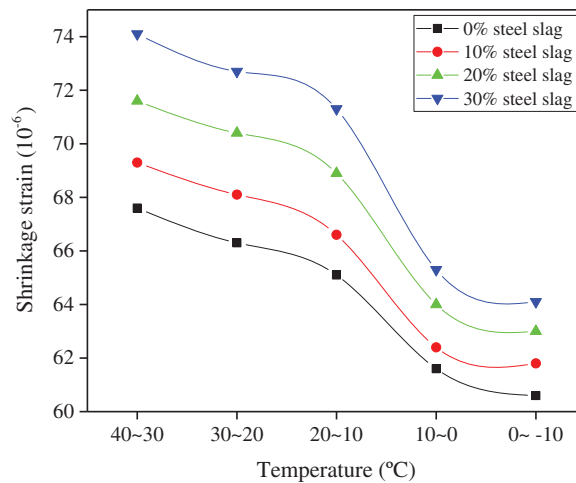
Figure 10: Temperature shrinkage strain of CMS with different steel slag contents

3.4.2 With Different Cement Contents

Fig. 11 illustrates the temperature shrinkage strain of CMS with different cement contents. It can be concluded that the shrinkage strain of CMS tended to be smaller as the temperature decreased. Besides, the higher the cement content, the more obvious the temperature shrinkage. Compared with the CMS with 4% cement, the temperature shrinkage strain of CMS with 5% and 6% cement increased by 10.9% and 18.3% respectively indicating that the influence of cement on temperature shrinkage was smaller. While the effect of cement content was more obvious than steel slag on the temperature shrinkage of CMS. This was because there were more active substances in the cement than in the steel slag, and more hydration products were produced by the hydration reaction.
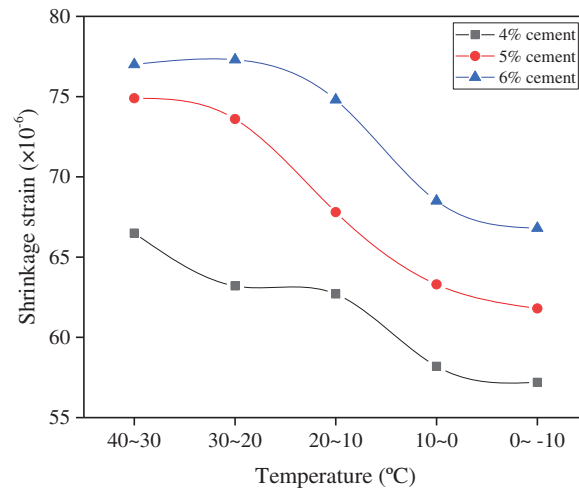
Figure 11: Temperature shrinkage strain of CMS with different cement contents

3.5 Dry-Temperature Shrinkage

The total shrinkage strain of CMS with different steel slag contents was presented in Fig. 12. With the increase of steel slag content, the total shrinkage strain of CMS decreased, and that with 0%, 10%, 20% and 30% steel slag was 365×10^{-6}, 320×10^{-6}, 295×10^{-6} and 273×10^{-6}, respectively. Thereafter, it could be concluded that the addition of steel slag could effectively reduce the total shrinkage and improve the shrinkage cracking resistance. As mentioned above, the hydration reaction of active material in steel slag increased the volume of products, thus compensating for the shrinkage deformation due to the change in water and temperature. Although the hydration reaction of active substances in steel slag increases the product content, the number of hydration products produced by steel slag was much less than that of cement. Therefore, the addition of steel slag had little effect on the dry-temperature shrinkage.
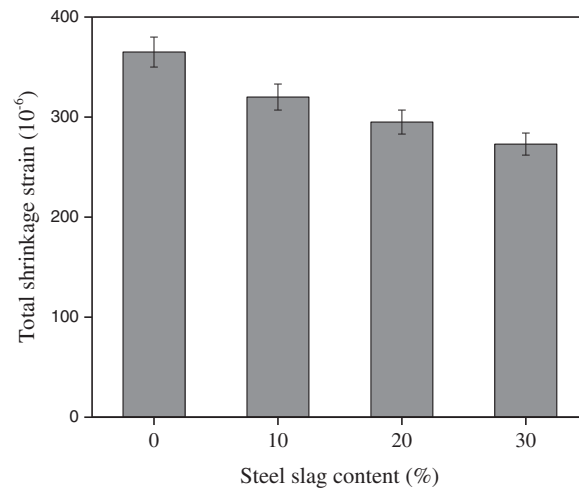
Figure 12: Total shrinkage strain of CMS with different steel slag contents

3.6 Analysis of Shrinkage Compensation Mechanism

3.6.1 XRD Images

The XRD images of steel slag at different hydration ages were given in Fig. 13. It is noteworthy that steel slag contains $Ca(OH)_2$, $CaCO_3$, C_3S, C_2S, f-CaO, RO phase and $Ca_2(Fe, Al)_2O_5$, etc. The characteristic peaks of C_3S, C_2S, RO phase, and $Ca_2(Fe, Al)_2O_5$ phase were higher, indicating that the contents of these substances were higher in the steel slag. With the increase in hydration time, the characteristic peaks of C_3S, C_2S, and f-CaO gradually decreased, while that of $Ca(OH)_2$ and $CaCO_3$ gradually increased. Therefore, it can be concluded that C_3S, C_2S, and f-CaO in steel slag have been hydrated to produce $Ca(OH)_2$ and $CaCO_3$, while $Ca_2(Fe, Al)_2O_5$, RO, and C_2F were not involved in the hydration reaction. Although cement contains C_3S and C_2S, the hydration reaction did not cause its volume expansion. Therefore, it could be considered that the hydration reactions of C_3S and C_2S were not the cause of the volume expansion of steel slag.
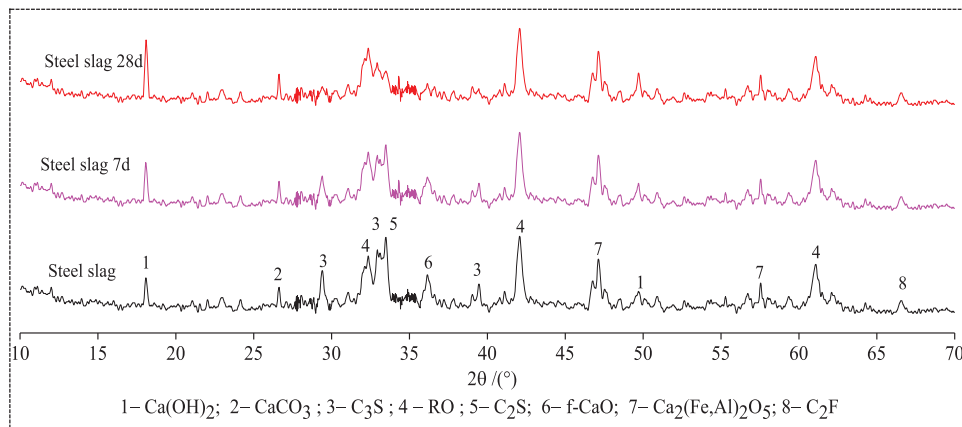
Figure 13: XRD images of steel slag at different hydration ages

Fig. 14 shows that there were no new characteristic peaks at 28 days of co-hydration of steel slag and cement, which implied that there were no new hydration products when steel slag and cement were co-hydrated compared with steel slag or cement alone. In addition, it was found that the characteristic peaks of the RO phase of the steel slag-cement hydration did not change much from those of the steel slag hydration alone, indicating that the RO phase was not involved in the hydration reaction. Therefore, it can be concluded that the main component causing the volume expansion of steel slag is f-CaO in the steel slag, and it was the volume expansion of $Ca(OH)_2$ produced by the hydration of f-CaO that offset and compensated for the volume shrinkage.

3.6.2 SEM Images

Fig. 15 gives the SEM images of steel slag at different hydration ages. As can be seen from Fig. 15a, white flocculated hydrated calcium silicate hydrate (C-S-H) and cubic $Ca(OH)_2$ were distributed on the surface of steel slag after 7 days of hydration reaction. C-S-H is gelatinous and does not show diffraction peaks in X-ray, so no characteristic peak of C-S-H was found in the XRD images. Besides, Fig. 15b showed the image of steel slag after 28 days of hydration reaction. It can be noted that the surface of steel slag was almost occupied by various hydration products, and therefore the surface of the original slag cannot be seen directly. Compared with the hydration products formed after 7 days, numerous hydration products especially scattered $Ca(OH)_2$ crystals piled up on the steel slag surface.

1– C_2F; 2– AFt; 3– $Ca(OH)_2$; 4– C_3S; 5– RO; 6– C_2S
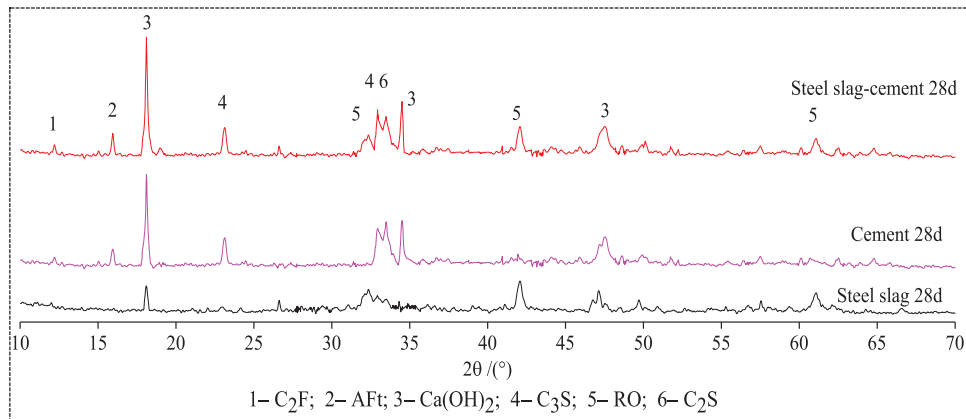
Figure 14: XRD images of each sample at 28 days of hydration reaction

(a) 7 d hydration reaction   (b) 28 d hydration reaction
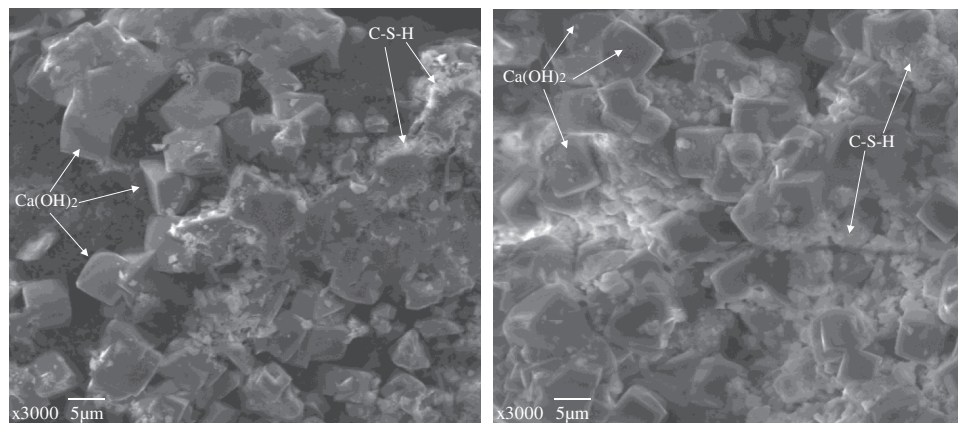
Figure 15: SEM images of steel slag at different hydration ages

Fig. 16 is the SEM images of cement and steel slag after 28 days of hydration reaction. As shown in Fig. 16a, the hydration products of cement contain $Ca(OH)_2$ in the form of irregular hexagonal sheet crystals, C-S-H in the form of wheat bundles and flocs, and calcium alumina (AFt) in the form of similar pine needles. Fig. 16b illustrates the hydration products of steel slag-cement after 28 days. The hydration products were mainly white flocculent C-S-H, needle-like AFt, and a large amount of accumulated $Ca(OH)_2$. Whereas $Ca(OH)_2$ produced by the hydration reaction of cement was mostly dispersed or aggregated, and that from steel slag-cement was densely packed. This is because the distribution of f-CaO in steel slag was relatively concentrated, so the $Ca(OH)_2$ from its hydration reaction was also aggregated and piled up with each other, increasing the volume of CMS. In addition, the images of XRD and SEM indicate that the hydration reactions of C_3S, C_2S, f-CaO, and other components in steel slag produced C-S-H and $Ca(OH)_2$. Among them, the hydration of f-CaO to form $Ca(OH)_2$ was the main reason for the volume expansion of steel slag and also the main material to compensate for the volume shrinkage of CMS.

(a) Cement   (b) Co-hydration of steel slag and cement
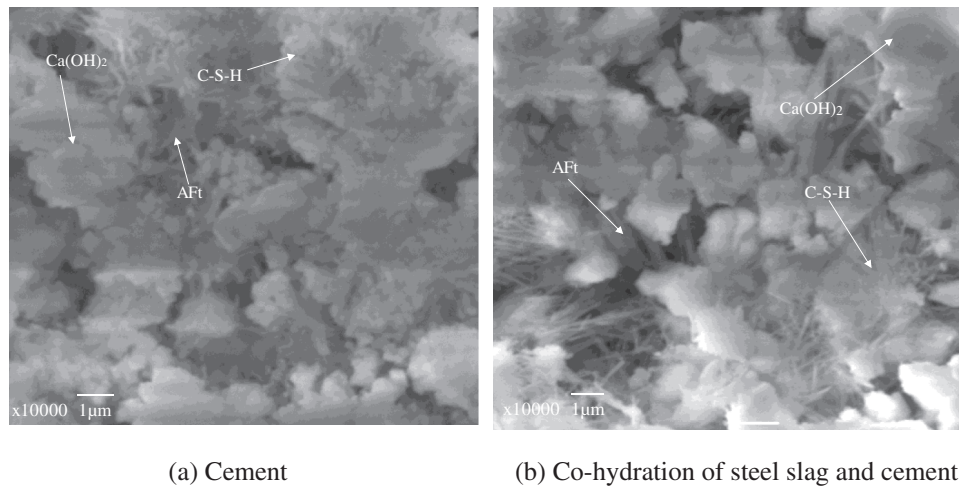
Figure 16: SEM images of cement and steel slag after 28 days hydration reaction

4 Conclusions

This study investigates the mechanical properties, shrinkage (dry shrinkage, temperature shrinkage, dry-temperature comprehensive shrinkage) and shrinkage-expansion mechanisms of CSMS with different steel slag and cement contents. Based on the experimental results, the following conclusions are drawn:

(1) The 7 d compressive strength of CSMS with 10%, 20% and 30% steel slag increase by 7.2%, 16.7% and 22.0% respectively. This is because the active substances in steel slag participate in the hydration reaction, and the products increase the denseness of CMS.

(2) The introduction of 20% steel slag in CSMS reduces the dry shrinkage by 21%, and increases temperature shrinkage by 5.8%, while the addition of cement increases the dry shrinkage and temperature shrinkage.

(3) On the aspect of dry-temperature comprehensive shrinkage, the addition of steel slag reduces the total shrinkage by 19.2% and improves its shrinkage cracking resistance.

(4) Compared with the hydration reaction of cement alone, the composite hydration reaction of steel slag with cement does not produce new hydrates. Among them, the hydration of f-CaO to form $Ca(OH)_2$ was the main reason for the volume expansion of steel slag and also the main material to compensate for the volume shrinkage of CSMS.

Conflicts of Interest: The authors declare that they have no conflicts of interest to report regarding the present study.

References

1. Andrade, H., Carvalho, J., Costa, L., Elói, F., Peixoto, R. (2021). Mechanical performance and resistance to carbonation of steel slag reinforced concrete. *Construction and Building Materials, 298(9),* 123910. DOI 10.1016/j.conbuildmat.2021.123910.

2. Nunes, V., Borges, P. (2021). Recent advances in the reuse of steel slags and future perspectives as binder and aggregate for alkali-activated materials. *Construction and Building Materials, 281(4),* 122605. DOI 10.1016/j. conbuildmat.2021.122605.

3. Xiang, X., Xi, J., Li, C., Jiang, X. (2016). Preparation and application of the cement-free steel slag cementitious material. *Construction and Building Materials, 114(7),* 874–879. DOI 10.1016/j.conbuildmat.2016.03.186.

4. Tang, G., Liu, X., Yang, Y., Chen, D., Zhang, H. et al. (2020). Phosphorus-containing silane modified steel slag waste to reduce fire hazards of rigid polyurethane foams. *Advanced Powder Technology, 31(4),* 1420–1430. DOI 10.1016/j.apt.2020.01.019.

5. Liu, J., Yu, B., Wang, Q. (2020). Application of steel slag in cement treated aggregate base course. *Journal of Cleaner Production, 269(10),* 121733. DOI 10.1016/j.jclepro.2020.121733.

6. Qiang, W., Meng, S., Jun, Y. (2016). Influence of classified steel slag with particle sizes smaller than 20 μm on the properties of cement and concrete. *Construction and Building Materials, 123(10),* 601–610.

7. Zhang, J., Ding, L., Li, F., Peng, J. (2020). Recycled aggregates from construction and demolition wastes as alternative filling materials for highway subgrades in China. *Journal of Cleaner Production, 255(5),* 120223. DOI 10.1016/j.jclepro.2020.120223.

8. Juan-Valdés, A., Rodríguez-Robles, D., García-González, J., Guerra-Romero, M., Morán-del, J. (2018). Mechanical and microstructural characterization of non-structural precast concrete made with recycled mixed ceramic aggregates from construction and demolition wastes. *Journal of Cleaner Production, 180(4),* 482–493.

9. Das, B., Prakash, S., Reddy, P., Misra, V. (2007). An overview of utilization of slag and sludge from steel industries. *Resources, Conservation and Recycling, 50(3),* 40–57. DOI 10.1016/j.resconrec.2006.05.008.

10. Barišić, I., Dimter, S., Rukavina, T. (2014). Strength properties of steel slag stabilized mixes. *Composites Part B: Engineering, 58(3),* 386–391.

11. Zhu, H., Ma, M., He, X., Zheng, Z., Su, Y. et al. (2021). Effect of wet-grinding steel slag on the properties of portland cement: An activated method and rheology analysis. *Construction and Building Materials, 286(6),* 122823. DOI 10.1016/j.conbuildmat.2021.122823.

12. Wu, S., Xue, Y., Ye, Q., Chen, Y. (2007). Utilization of steel slag as aggregates for stone mastic asphalt (SMA) mixtures. *Building and Environment, 42(7),* 2580–2585. DOI 10.1016/j.buildenv.2006.06.008.

13. Guo, J., Bao, Y., Wang, M. (2018). Steel slag in China: Treatment, recycling, and management. *Waste Management, 78(8),* 318–330. DOI 10.1016/j.wasman.2018.04.045.

14. Roslan, N., Ismail, M., Abdul-Majid, Z., Ghoreishiamiri, S., Muhammad, B. (2016). Performance of steel slag and steel sludge in concrete. *Construction and Building Materials, 104(2),* 16–24. DOI 10.1016/j.conbuildmat.2015.12.008.

15. Subathra, D., Madhan Kumar, M., Iswarya, N., Gnanavel, B. (2020). Durability of steel slag concrete under various exposure conditions. *Materials Today: Proceedings, 22(4),* 2764–2771.

16. Maslehuddin, M., Sharif, A., Shameem, M., Ibrahim, M., Barry, M. (2003). Comparison of properties of steel slag and crushed limestone aggregate concretes. *Construction and Building Materials, 17(3),* 105–112. DOI 10.1016/ S0950-0618(02)00095-8.

17. Netinger, I., Bjegovic, D., Vrhovac, G. (2011). Utilisation of steel slag as an aggregate in concrete. *Materials and Structures, 44(4),* 1565–1575. DOI 10.1617/s11527-011-9719-8.

18. Wang, G., Wang, Y., Gao, Z. (2010). Use of steel slag as a granular material: Volume expansion prediction and usability criteria. *Journal of Hazardous Materials, 184(1–3),* 555–560. DOI 10.1016/j.jhazmat.2010.08.071.

19. Liao, X., Xiao, F., Chen, Z., Xing, L. (2012). The influence of different subbase materials on the crack of cement stabilized macadam base during construction. *Advanced Materials Research, 591–593,* 955–959. DOI 10.4028/ www.scientific.net/AMR.591-593.955.

20. You, L., Yue, Y., Yan, K., Zhou, Y. (2021). Characteristics of cement-stabilized macadam containing surface-treated recycled aggregates. *Road Materials and Pavement Design, 22(9),* 1–15. DOI 10.1080/14680629.2020.1740771.

21. Du, S. (2019). Mechanical properties and shrinkage characteristics of cement stabilized macadam with asphalt emulsion. *Construction and Building Materials, 203(4),* 408–416. DOI 10.1016/j.conbuildmat.2019.01.126.

22. Martins, A., de Carvalho, J., Costa, L., Andrade, H., de Melo, T. et al. (2021). Steel slags in cement-based composites: An ultimate review on characterization, applications and performance. *Construction and Building Materials, 291(7),* 123265. DOI 10.1016/j.conbuildmat.2021.123265.

23. Li, Z., Zhang, S., Liang, X., Ye, G. (2020). Cracking potential of alkali-activated slag and fly ash concrete subjected to restrained autogenous shrinkage. *Cement and Concrete Composites, 114(11),* 103767. DOI 10.1016/j.cemconcomp.2020.103767.

24. Li, W., Lang, L., Lin, Z., Wang, Z., Zhang, F. (2017). Characteristics of dry shrinkage and temperature shrinkage of cement-stabilized steel slag. *Construction and Building Materials, 134(3),* 540–548. DOI 10.1016/j. conbuildmat.2016.12.214.

25. Qasrawi, H. (2014). The use of steel slag aggregate to enhance the mechanical properties of recycled aggregate concrete and retain the environment. *Construction and Building Materials, 54(3),* 298–304. DOI 10.1016/j. conbuildmat.2013.12.063.

26. Xin, Y., Zhong, T., Song, T., Zhu, P. (2016). Performance of concrete made with steel slag and waste glass. *Construction and Building Materials, 114(7),* 737–746.

27. Baalamurugan, J., Kumar, V., Chandrasekaran, S., Balasundar, S., Venkatraman, B. et al. (2021). Recycling of steel slag aggregates for the development of high density concrete: Alternative & environment-friendly radiation shielding composite. *Composites Part B: Engineering, 216(7),* 108885. DOI 10.1016/j.compositesb.2021.108885.

28. Miah, M., Ali, M., Lo Monte, F., Paul, S., Babafemi, A. et al. (2021). The effect of furnace steel slag powder on the performance of cementitious mortar at ambient temperature and after exposure to elevated temperatures. *Structures, 33(10),* 2811–2823.

29. Xiao, B., Wen, Z., Miao, S., Gao, Q. (2021). Utilization of steel slag for cemented tailings backfill: Hydration, strength, pore structure, and cost analysis. *Case Studies in Construction Materials, 15(12),* e00621. DOI 10.1016/j.cscm.2021.e00621.

30. El-Didamony, J., Helmy, I., Ali, H. (2011). Utilization of an industrial waste product in the preparation of low cost cement. *The Journal of American Science, 7(9),* 527–533.

31. Biskri, Y., Achoura, D., Chelghoum, N., Mouret, M. (2017). Mechanical and durability characteristics of high performance concrete containing steel slag and crystalized slag as aggregates. *Construction and Building Materials, 150(9),* 167–178. DOI 10.1016/j.conbuildmat.2017.05.083.

32. Lim, S., Cheah, C., Ramli, M. (2019). The setting behavior, mechanical properties and drying shrinkage of ternary blended concrete containing granite quarry dust and processed steel slag aggregate. *Construction and Building Materials, 215(8),* 447–461. DOI 10.1016/j.conbuildmat.2019.04.162.